Nanometer-Scale Ion Aggregates in Aqueous Electrolyte Solutions: Guanidinium Carbonate

P. E. Mason,[†] G. W. Neilson,[‡] Steve R. Kline,[||] C. E. Dempsey,[§] and J. W. Brady*,[†]

Department of Food Science, Stocking Hall, Cornell University, Ithaca, New York 14853, H. H.Wills Physics Laboratory, University of Bristol, Bristol BS8 1TL, United Kingdom, Department of Biochemistry, University of Bristol, Bristol BS8 1TD, United Kingdom, and Center for Neutron Research, National Institute of Standards and Technology, 100 Bureau Drive, Mail Stop 8562, Gaithersburg, Maryland 20899

Received: December 9, 2005; In Final Form: April 19, 2006

Neutron diffraction with isotopic substitution (NDIS) experiments and molecular dynamics (MD) simulations have been used to characterize the structure of aqueous guanidinium carbonate (Gdm_2CO_3) solutions. The MD simulations found very strong hetero-ion pairing in Gdm_2CO_3 solution and were used to determine the best structural experiment to demonstrate this ion pairing. The NDIS experiments confirm the most significant feature of the MD simulation, which is the existence of strong hetero-ion pairing between the Gdm^+ and CO_3^{2-} ions. The neutron structural data also support the most interesting feature of the MD simulation, that the hetero-ion pairing is sufficiently strong as to lead to nanometer-scale aggregation of the ions. The presence of such clustering on the nanometer length scale was then confirmed using small-angle neutron scattering experiments. Taken together, the experiment and simulation suggest a molecular-level explanation for the contrasting denaturant properties of guanidinium salts in solution.

Introduction

Electrolyte solutions are of fundamental importance in problems ranging from batteries to living cells. They are particularly important in biology, where most processes take place in salt solutions (e.g., blood plasma, cellular cytoplasm, etc.). Apart from governing the osmotic state of such systems, it is well-known that some ions can significantly affect such thermodynamic equilibria as protein folding and unfolding or the binding of ligands to proteins. The familiar Hofmeister series, first characterized more than a century ago,[1] ranks the various cations and anions in terms of their effects on protein conformational stability and solubility. The mechanisms underlying the Hofmeister series have been the subject of much investigation,[2−4] but particularly for molecular ions there remain unresolved questions about what governs their relative ordering. It has long been believed, however, that the way in which the ions interact with each other and with water plays a major role and understanding the microscopic structure and dynamics of such systems will be crucial to understanding their macroscopic properties.

Characterizing the structural organization of liquid solutions has proven to be a difficult problem. Most experimental techniques provide only indirect information.[5,6] The most effective direct structural experimental probe has been neutron diffraction experiments. When combined with the technique of isotopic substitution of specific atoms in paired or grouped experiments, such studies have been extremely powerful.[7,8] In the case of complex molecular solutes with several different atom types, however, the scattering data can be difficult to interpret. For such systems, the rich detail of molecular dynamics (MD) simulations can be used to help interpret the complex neutron scattering seen in the diffraction experiments.

Previous studies have reported the combination of neutron diffraction with isotopic substitution (NDIS) experiments and MD simulations to characterize the structuring of aqueous solutions of guanidinium chloride,[9] guanidinium thiocyanate, and guanidinium sulfate.[10] The study of guanidinium sulfate found hetero-ion pairing of sufficient strength and extent for the sulfate salt as to suggest the formation of nanometer-scale aggregates in ionic solutions. These studies found significant solvent structuring around guanidinium ions (Gdm^+) and experimental evidence for strong hetero-ion pairing (even at modest concentrations) as well as indirect and computational evidence for homo-ionic guanidinium pairing in a manner that resembles hydrophobic stacking. The nature of these interactions varies with the charge and shape of the ions and helps to explain the Hofmeister behavior of these species. In the case of the guanidinium sulfate, the strength and geometry of the interactions between the Gdm^+ and sulfate ions led to nanometer-scale aggregation of the ions. The mode of interaction between these two ions involved mainly double hydrogen bonds between the O−S−O and the HN−C−NH motifs in ways that allowed each to participate in additional pairings, which led to networks of associated ions. On the basis of the anionic structure, it would seem reasonable to assume that similar ionic pairing could occur in guanidinium carbonate solutions. Furthermore, the aggregation might be expected to be even stronger since the −2 charge is spread over only three oxygen atoms rather than four as in sulfate. The present paper describes similar coupled NDIS experiments and MD simulations of aqueous guanidinium carbonate (Gdm_2CO_3) solutions designed to test this hypothesis. These studies also found evidence for strong ion pairing and the potential for the formation of mesoscale aggregates. A subsequent small-angle neutron scattering (SANS) experiment was then used to demonstrate the presence of such nanometer-

* Author to whom correspondence should be addressed. Phone: +1 607 255-2897. Fax: +1 607 254-4868. E-mail: jwb7@cornell.edu.
[†] Cornell University.
[‡] H. H.Wills Physics Laboratory, University of Bristol.
[§] Department of Biochemistry, University of Bristol.
[||] National Institute of Standards and Technology.

10.1021/jp0572028 CCC: $33.50
Published on Web 06/21/2006

scale structures in the Gdm_2CO_3 solution but their absence in GdmCl solutions, as predicted by the MD simulations.

Neutron diffraction with isotopic substitution experiments, which exploit the differences in scattering cross sections for different atomic isotopes, are limited to some extent in their application to many biological solutes due to several circumstances. The most problematic of these difficulties is that exchangeable hydrogen atoms cannot be labeled due to their labile nature; all of the hydrogen atoms in the guanidinium ion are in this category. The carbonate anion contains only carbon and oxygen atoms, and neither of these elements exhibits sufficient contrast in neutron scattering length to be used in a viable NDIS experiment. It is thus not possible to exploit NDIS techniques to probe the structuring of solvent around the carbonate ion. The same problem applies to the carbon atom of the guanidinium ion. The only atom type in Gdm_2CO_3 suitable for this type of experiment is the nitrogen of the guanidinium. Hydrogen and deuterium have coherent neutron scattering lengths of -3.74 and 6.67 fm, respectively. For water it is therefore possible to make a mixture of isotopes such that the average coherent neutron scattering length of hydrogen is 0.00 fm (such a mixture will be hereafter referred to as "null water"). In such a solution no correlations to hydrogen are visible. When this situation is exploited, it is possible to devise an experiment that probes the solution structure around the nitrogen atoms of the guanidinium ions.

Methods

Computational Procedures. In the MD simulations a neutral periodic cubic system was created at 1.5 *m* concentration containing a number of independent guanidinium cations and carbonate counterions surrounded by explicit water molecules. The simulations employed the same revised CHARMM22 guanidinium potential energy function used in our previous studies,[9,10] with the atomic partial charges assigned symmetrically (atom charges: C, 0.64; N, -0.80; H, 0.46). The atomic charges and structure for the carbonate ions were calculated using GAMESS[11] at the MP2/6-311G** level using Mulliken population assignment, giving partial charges of C, 0.676, and O, -0.892. Water molecules were represented using the TIP3P model.[12] All simulations were performed using the CHARMM program,[13] with chemical bonds to hydrogen atoms kept fixed using SHAKE[14] and a time step of 1 fs. Arbitrary starting coordinates were generated by randomly placing and orienting 48 Gdm molecules and 24 carbonate ions in a cubic box with sides of 34 Å. These coordinates were superimposed on a box of 1296 water molecules, and those that overlapped any solute heavy atom were discarded. By design this procedure produced a 1.5 *m* solution (24 Gdm_2CO_3 in 889 TIP3P water molecules, 1.500 *m*). Finally, the box length was rescaled to 31.7840 Å; this yielded the correct physical number density (0.101 atoms $Å^{-3}$).

Van der Waals interactions were smoothly truncated on an atom-by-atom basis using switching functions[13] from 10.5 to 11.5 Å, while electrostatic interactions were treated using the Ewald method[15] with a real space cutoff of 12.5 Å, $\kappa = 0.333$, and a K_{max}^2 of 27. Initial velocities were assigned from a Boltzmann distribution (300 K) followed by 5 ps of equilibration dynamics with velocities being reassigned every 0.1 ps. The simulation was then run for 4.5 ns with no further velocity reassignment. The first 1.5 ns of this were taken as equilibration, and the remaining 3 ns were used for analysis. Subsequently, experimentally measurable values were obtained by summing the calculated pair correlation functions, weighted by the scattering prefactors shown in Table 1. To test the sensitivity of the results this procedure was repeated but with a different set of starting coordinates and velocity assignments, with the simulation run as before for 2 ns. Another 2 ns simulation at one-third the concentration was conducted for 16 guanidinium and 8 carbonate ions in 889 water molecules, for a concentration of 0.50 M, to test the concentration dependence.

TABLE 1: Scattering Prefactors

		A	*B*	*C*	
prefactor	$g_{ND}(r)$	$g_{NO}(r)$	$g_{NN}(r)$	$g_{CN}(r)$	total
${}^nG_N(r)$ (D_2O)	11.03	4.46	0.91	0.38	16.78
${}^nG_N(r)$ (null)		4.46	0.91	0.38	5.75

Neutron Diffraction with Isotopic Substitution Experiments

Sample Preparation. All the light water used in this experiment had a resistivity of 18 MΩ cm and is referred to hereafter as pure water. A 15 mm diameter column was loaded with 15 g of Dowex 1 × 8 Cl ion-exchange resin. An 80 mL aliquot of 10 M NaOH was eluted down this column, followed by a washing with 100 mL of pure water (such that no further NaOH was being eluted from the column). GdmCl (610 mg, 6.39 mmol) was dissolved into 3 mL of pure water and washed onto the column. This was then eluted with pure water to directly and exactly fill a 50 mL volumetric flask. A 2.00 mL sample of this guanidine solution was taken and diluted up to about 20 mL with pure water (the solution pH was 12.16) and was potentiometrically titrated versus HCl (0.025012 M). This gave an overall yield for the conversion of GdmCl to guanidine of 93%. Test runs of this experiment showed that yields in the mid-90% range were typical and that the eluant contained only enough chloride to produce a slight haze with $AgNO_3$ solution. To the remaining 48 mL of guanidine solution carbonated water (75 mL, ~0.045 M) was added to adjust the pH of the solution to 6.2. This solution was stirred for an additional hour before the water was removed using a rotary evaporator, and the solid was well dried at 70 °C under vacuum. The Gdm_2CO_3 was then transferred to a glass ampule, and the water was removed under high vacuum. Null water (3 mL) was added and again removed under high vacuum. This process was repeated a further two times before the correct amount of null water was added. The null water in this experiment was composed of 84.506 g of pure water and 52.595 g of D_2O (99.9 at. % D). The correct amount of null water was then added to effect a molar ratio of 1.5 mol Gdm_2CO_3 to 55.555 mol of water (referred to in this paper as a 1.5 *m* solution) while maintaining a high vacuum before the ampule was sealed under high vacuum. The ampule was only opened immediately prior to the transfer of the solution to the sample container used in this experiment. This method was also used for the production of the $^{15}N_3$-guanadinium carbonate solution.

Data Analysis. The difference methods of NDIS are well established in the literature;[7,8,16] only those parts that are relevant to the present work are reproduced here. The main tenet of the method is that there is complete isomorphism between isotopically labeled samples of the same chemical compound. Total neutron scattering patterns were obtained for 1.50 *m* solutions of $^{15}N_3$-Gdm_2CO_3 and $^{nat}N_3$-Gdm_2CO_3, (in null water) on the D4C diffractometer at the Institut Laue-Langevin (ILL), Grenoble, France, corrected for multiple scattering and absorption,[17] and normalized versus a standard vanadium rod to give the $F(Q)$

values of the respective solutions. $F(Q)$ can be written as

$$F(Q) = \sum_{\alpha}\sum_{\beta} c_\alpha c_\beta b_\alpha b_\beta (S_{\alpha\beta}(Q) - 1) \quad (1)$$

where c_α is the atomic concentration of species α whose neutron coherent scattering length is b_α, and the sums are over all four atomic species in the solution, which in order of concentration are H, O, N, and C. $S_{\alpha\beta}(Q)$ is the partial structure factor of atoms α and β and is directly related to the radial pair distribution function $g_{\alpha\beta}(r)$ through Fourier transformation

$$g_{\alpha\beta}(r) - 1 = \frac{1}{2\pi^2\rho r}\int (S_{\alpha\beta}(Q) - 1)Q \sin(Qr)\, dQ \quad (2)$$

Through the use of the first-order difference method of NDIS upon these two patterns, the difference function ${}^n\Delta_N(Q)_{null}$ was obtained. This function provides information associated with correlations between nitrogen atoms and all other atom types other than hydrogen (which has a prefactor of zero due to the average coherent scattering length of H in null water being zero) and can be written as

$${}^n\Delta_N(Q)_{null} = \frac{AS_{NO}(Q) + BS_{NN}(Q) + CS_{NC}(Q)}{A + B + C} - 1 \quad (3)$$

The superscript *n* indicates that this function is dimensionless, having been normalized by division by the sum of the scattering prefactors, in this case $A + B + C$. The prefactors themselves (Table 1) are composed of a product of $c_\alpha c_\beta b_\alpha \Delta b_N$, where $\Delta b_N = b^{15}_N - b^{nat}_N$. The Fourier transform of this function, ${}^nG_N(r)_{null}$, provides information on the pairwise structural correlations between nitrogen atoms and all atoms other than hydrogen atoms in the system. Specifically

$${}^nG_N(r)_{null} = \frac{Ag_{NO}(r) + Bg_{NN}(g) + Cg_{NC}(r)}{A + B + C} - 1 \quad (4)$$

${}^nG_N(r)_{null}$ as measured by experiment and calculated from the MD simulation is shown in Figure 1.

SANS Experiments. Small-angle neutron scattering experiments were performed on the NG3 30 m SANS instrument[18] at the National Institute of Standards and Technology Center for Neutron Research in Gaithersburg, MD. (The SANS reduction and analysis software are freely available at http://www.ncnr.nist.gov/programs/sans/manuals/red_anal.html.) Solutions of 3 M GdmCl (Aldrich 99+%) and 1.5 M Gdm_2CO_3 (Aldrich 99%) were prepared by direct dissolution of the natural-abundance salts into D_2O (99.9% D, Cambridge Isotope Labs, Cambridge, MA; the mention of trade names does not imply endorsement by NIST). Note that all of the hydrogen atoms in these systems are exchangeable. To remove dust the solutions were filtered through surfactant-free cellulose acetate filters (Nalgene) of 0.2 μm pore size. Neutrons of wavelength $\lambda = 6$ Å with a distribution of $\Delta\lambda/\lambda = 15\%$ were incident on samples held in 5 mm path length quartz cells. The sample-to-detector distance was chosen to give an overall q-range of 0.014 $Å^{-1} < q < 0.44$ $Å^{-1}$, where $q = (4\pi/\lambda)\sin(\theta/2)$ is the magnitude of the scattering vector. Sample scattering was corrected for background and empty cell scattering, and the sensitivity of individual detector pixels was normalized. The corrected data sets were circularly averaged and placed on an absolute scale of cm^{-1} using direct beam transmission measurements.

Since there is no accepted literature method for making multiple scattering corrections on the incoherent portion of the data, such corrections were not attempted. While this means that the data ultimately does not achieve the theoretically expected low-Q limit, this is not a significant factor since the incoherent scattering is structureless (flat), so that the correction to these data is also structureless. Furthermore, it should be stressed that any such correction would be almost identical for both solutions, given the nearly identical atomic composition of these two solutions. It is therefore not possible to ascribe the qualitatively very different SANS results for these two solutions, described below, to multiple scattering.

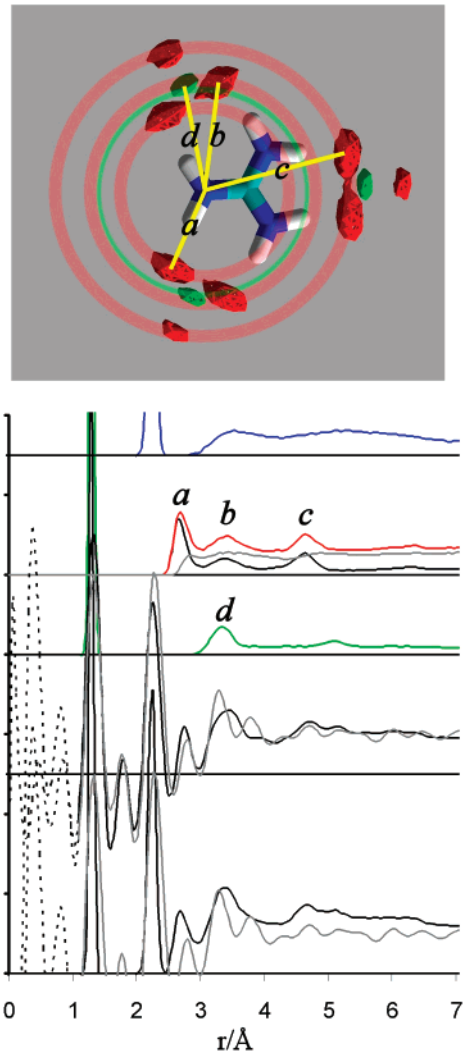

Figure 1. Upper panel: Contour map of the density of CO_3^{2-} around the Gdm^+ ion (red and green for O and C on carbonate, respectively, at density contours of 65 times the number density of each atom). From the density map the double hydrogen bond form of the interaction between Gdm^+ and CO_3^{2-} is clear. Shown as red and green concentric rings are the correlations from the substituted nitrogen to ion-paired carbonate ions. Lower panel: Experimental and MD predictions for ${}^nG_N(r)_{null}$. The structure factors from bottom to top are: bottom, black, the MD prediction for ${}^nG_N(r)_{null}$; bottom, gray, the experimentally determined ${}^nG_N(r)_{null}$; lower-middle, same as the bottom plot except that the experimental resolution has been applied to the MD data; middle, green, the NC component of ${}^nG_N(r)_{null}$; upper-middle, red, the total NO component in ${}^nG_N(r)_{null}$ (This has been further split into the components for NO_{water} (gray) and $NO_{carbonate}$ (black). This split clearly highlights that despite the fact that only 7% of the oxygen atoms are on the carbonate ion, they constitute the dominant nuclei surrounding the Gdm^+ ion.); upper, the NN component of ${}^nG_N(r)_{null}$.

The measured small-angle signal is dependent upon the number of clusters, the difference in scattering length density between those clusters and the solvent, and the size and shape of the clusters. In the current case the scattering lengths of both

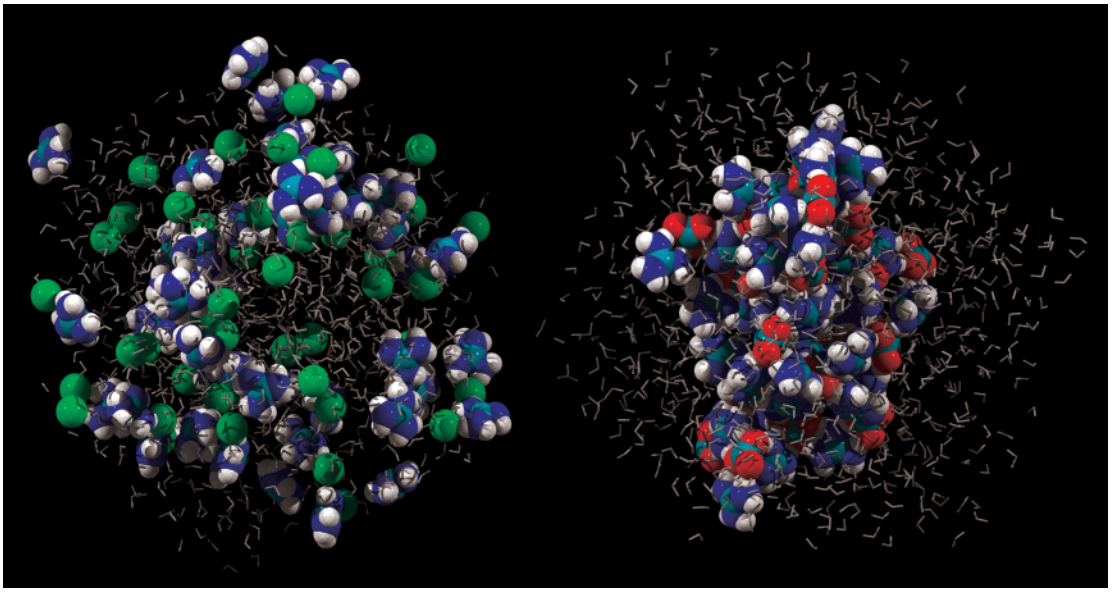

Figure 2. Snapshot of the MD simulation of 1.5 *m* Gdm_2CO_3 and 3 *m* GdmCl (both containing identical concentrations of Gdm^+). Clearly visible in the right panel is the long-range aggregation of Gdm^+ and CO_3^{2-} ions.

the water and ions are similar (5.4 fm for water and 6.9 and 6.5 fm for GdmCl and Gdm_2CO_3, respectively). However, the molecular ions have high local number densities (for instance, the Gdm^+ ion has 10 nuclei in a relatively small volume compared to the volume occupied by 10 water nuclei), and it is expected that this will be the most significant contribution to the differential scattering length density observed in the Gdm_2CO_3 solution.

Results and Discussion

As had been expected, the guanidinium and carbonate ions in the MD simulations were found to pair strongly. The ion pairing results in ion clusters in the solution on the 1.5 nm length scale. From the trajectory coordinate sets the predicted function ${}^nG_N(r)_{null}$ was calculated and is displayed in Figure 1. An advantage of simulations over experimental determination of this function is that the calculated ${}^nG_N(r)_{null}$ can be resolved into its component correlations, NC, NO, and NN, which are also displayed in Figure 1. In addition, the explicit knowledge of positions of all atoms in the simulations allows the calculation of the complete anisotropic atomic distribution function for carbonate around the guanidinium ions, which is shown in Figure 1. This figure also illustrates the origin of each intermolecular peak in the atomic pair radial distribution functions in terms of the geometric relationship between regions of high atomic density and the guanidinium atomic positions.

Figure 2 illustrates the ion association in a typical snapshot taken from the trajectory, which is also shown in a movie included in the Supporting Information. The clustering observed in these simulations was not an accident of the initial starting conditions, since the repeat of the simulation with different starting positions for the ions and different assignments of initial velocities produced the same clustering. As in a related Gdm_2SO_4 simulation[10] the time scale required for this aggregation was on the order of 1 ns. The results were also not strongly concentration-dependent, since the repeat of the simulation at 0.50 M also produced ion aggregation. Also as in the Gdm_2SO_4 case, the structure of these aggregates did not suggest the formation of a new phase, and all ions in the cluster remained in direct contact with the aqueous solvent (that is, there is no interior). This behavior differed from incipient phase separation, since there was no tendency for the cluster to become more spherical, with an interior composed of the new phase segregated from the water. The extent of the aggregation was almost total; averaged over the final 3 ns, 100% of the carbonate ions were bound in such clusters, using a 4.4 Å cutoff radius (the position of the first minimum in the guanidinium carbon−carbonate carbon radial distribution function). Similarly, only 0.7% of the guanidinium ions were not bound in the clusters during the simulations.

Although the simulation results seem reasonable on geometric grounds, there has been little or no previous experimental evidence to suggest that such mesoscopic-scale structuring occurs in aqueous solutions. The results thus stand as a prediction to be tested by experiment. To test this prediction a set of NDIS experiments on Gdm_2CO_3 was also performed.

Two different experiments were examined for their feasibility and usefulness in characterizing ion structure in Gdm_2CO_3 solutions. One involved performing the NDIS $^{15}N/^{nat}N$ substitution in 1.5 *m* Gdm_2CO_3 in water where exchangeable hydrogen atoms are deuterium (${}^nG_N(r)_{D_2O}$, Figure 3), and the other involved performing the same experiment on a solution where the average coherent scattering length of hydrogen is zero (${}^nG_N(r)_{null}$, Figure 1). The scattering prefactors (the weighting factors for the $g(r)$ values measured in this experiment) for both experiments, as calculated from the coherent scattering lengths of the nuclei in question and their atomic concentrations, are shown in Table 1.

The results of the MD simulations were used to predict the usefulness of these two experiments with respect to their ability to detect the strong ion pairing suggested by the modeling. Traditionally NDIS experiments have been performed so as to provide the best contrast (in this case the experiment in D_2O). However, the MD simulations show that for the current case the extra contrast obtained by performing the experiment in D_2O simply diminishes or helps to conceal the signal due to the ion pairing (Figure 3). Specifically, the intramolecular peaks in $g_{NH}(r)$ at 2.5 and 3.1 Å conceal the two key signatures of ion pairing, namely, the peaks in $g_{NO}(r)$ and $g_{NC}(r)$ at 2.8 and 3.3 Å, respectively. Thus, for comparison with the MD results, the more challenging null water NDIS experiment with the lower contrast is of more use than the higher contrast D_2O experiment.

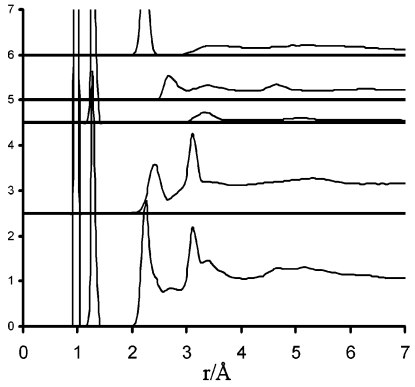

Figure 3. Function ${}^{n}G_{N}(r)_{D_2O}$ and its components as calculated from the MD simulation of 1.5 *m* Gdm_2CO_3. The bottom curve is ${}^{n}G_{N}(r)_{D_2O}$. The upper four curves are the contributions to this function from (bottom to top) the NH, NC, NO, and NN correlations. The key features that demonstrate ion pairing and nanometer-scale structure are the peaks in the NC and NO components at 3.3 and 2.8 Å, respectively, and the augmentation in the function ${}^{n}G_{N}(r)_{D_2O}$ in the region about 3.5 Å. Both of these features are obscured by the NH correlation, making this experiment a poor choice for the demonstration of ion pairing in Gdm_2CO_3 despite having 3 times the contrast of the same experiment performed in null water.

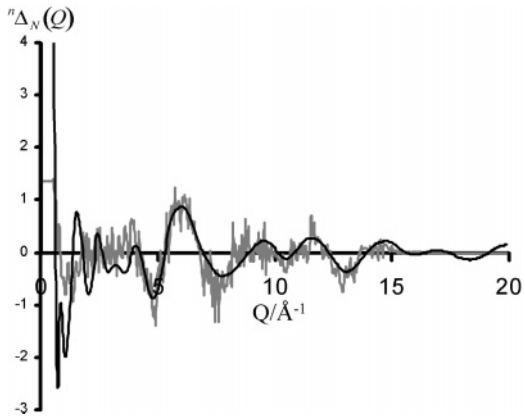

Figure 4. Directly measured experimental function ${}^{n}\Delta_{N}(Q)_{null}$ (gray) and the same function calculated from the MD simulation (black). It is demonstrable that virtually all of this function above 5 $Å^{-1}$ is due to intramolecular correlations within the Gdm^+ ion (the NC and NN correlations). The nanometer-scale structure observed in the MD simulation is represented by the very large increase in ${}^{n}\Delta_{N}(Q)_{null}$ below 0.5 $Å^{-1}$. While this is below the range of the current experimental data, the sharp rise in the data just before this cutoff is suggestive that there may indeed be a large small-angle signal present. The fact that the MD shows that there are significant features above 16 $Å^{-1}$ means that the intramolecular correlation in the experimental measurement will be somewhat resolution-limited.

Figure 4 displays the difference function ${}^{n}\Delta_{N}(Q)_{null}$ defined in eq 3 as calculated from the experimental data and the MD simulations. This is perhaps the most useful comparison that can be made between the experimental and the simulation results. To interpret this comparison it is useful to recall several general features of the relationship between the *Q*-space and the *r*-space functions. The intramolecular correlations seen in Figure 1 at 1.3 and 2.3 Å (due to the NC and NN correlations within the guanidinium ion) are manifested in the *Q*-space data as relatively lightly damped sinelike functions with wavelengths of ~4.0 and 2.3 $Å^{-1}$. These intramolecular correlations demonstrably account for almost all of the function ${}^{n}\Delta_{N}(Q)_{null}$ above about 5 $Å^{-1}$, where the fit between the experimental data is good to excellent. It should further be noted that in the MD results there are oscillations in ${}^{n}\Delta_{N}(Q)_{null}$ above 16.5 $Å^{-1}$, the experimental limit of the D4C diffractometer using a neutron wavelength of 0.7 Å. This fact means that the experimental structure obtained for the intramolecular correlations will be somewhat resolution-limited. The longer-range structure is manifested by much more severely damped, higher-frequency oscillations in *S*(*Q*) (which have decreased to essentially 0 by 5 $Å^{-1}$), although this is convoluted by molecular correlations that also have significant frequency components in this range. The larger the *r*-space structure that is represented, the more severe the damping, and the higher the frequency of the oscillations in *S*(*Q*). The comparison between the experimental measurement and the MD prediction in the region 0−5 $Å^{-1}$ is good, but most significantly, the experimental structure shows signs of a significant small-angle peak below the low-*Q* cutoff of the D4C diffractometer (~0.55 $Å^{-1}$). The most significant feature of these data is that the key signature of mesoscopic structuring of ions in the solution is present in ${}^{n}\Delta_{N}(Q)_{null}$.

The Fourier transformation of *Q*-space data to *r*-space data involves a compromise between the resolution and the reduction of "ringing". If the entire data range is transformed, then the best resolution is obtained, giving the best representation of the data (Figure 1). However, while the intermolecular correlations are defined at the experimental limit, the data tends to exhibit a ringing at higher *r*-values due to termination errors in the Fourier transform (FT). It is therefore common to reduce the high-*Q* limit of the data range used in the FT. This approximation has the positive effect of reducing the ringing at the cost of lowering the maximum obtainable resolution. The experimental ${}^{n}G_{N}(r)_{null}$ has a significantly smaller value in the range 3−20 Å than the MD function. This is due in part to the low-*Q* cutoff of the experimental data (0.55 $Å^{-1}$). The more relevant comparison between the experimental and the MD functions, where the *Q*-space MD data was Fourier transformed using the same *Q*-range as the experimental data (imposing the experimental resolution limits on the MD data), is also shown in Figure 1. It is important to note the very good agreement between the MD and the NDIS data, when both data sets are transformed with the experimental limits, and the significant difference that exists between the two when the experimental limits are not forced on the MD data. This latter observation particularly applies to the peak due to the NO correlation at 2.8 Å. This difference is an intrinsic problem with the NDIS data, which does not have a sufficiently large *Q*-range to accurately represent a molecular correlation. The FT of this peak will contain rippling on either side of the peak. This rippling interferes with the NO correlation at 2.8 Å. It should be noted that given certain *Q*-ranges it may not be physically possible to describe the *r*-space data accurately, most specifically when interpreting features adjacent to intramolecular correlations. In general, all of the peaks associated with hetero-ion pairing are observed in the experimental function (the peaks at 2.8, 3.2, and 4.8 Å), although they do not appear to be as strong in the NDIS measurement as they do in the MD prediction. The ${}^{n}G_{N}(r)_{null}$ function calculated from the previous MD simulations of GdmCl,[9] where the hetero-ion pairing is much weaker, does not display any features above 2.9 Å (Figure 5). The peaks in the regions 2.8, 3.2, and 4.8 Å are descriptive and characteristic of strong hetero-ion pairing between the guanidinium and carbonate ions. Furthermore, the NO correlation observed at 2.8 Å is significantly shorter than that measured in the experiment. This observation is important and reflects the van der Waals radius for the oxygen atoms in the carbonate ions being too small by about 0.1 Å. This observation would also explain why the hetero-ion pairing is substantially stronger in the MD simulations than in the experimental measurement. More

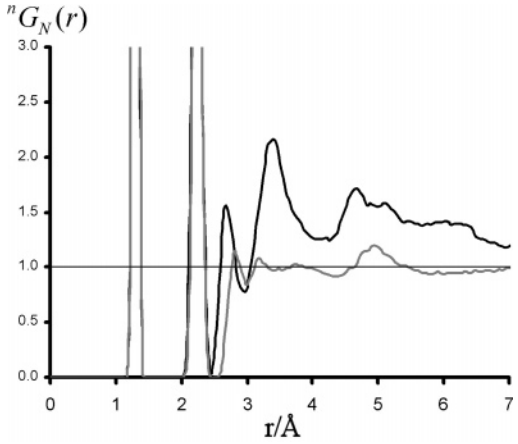

Figure 5. To highlight the clarity with which these measurement represent ion pairing, the function $^nG_N(r)_{null}$ shown as calculated from MD simulations of 3 *m* GdmCl solution (gray)[9] and 1.5 *m* Gdm_2CO_3 (black), with hetero-ion pairing being relatively weak in the former and greatly stronger in the latter. Both solutions have the identical concentration of Gdm^+.

unclear is the origin of the splitting of the peak around 3.5 Å in the NDIS data, since only a single broad feature is observed for the MD prediction. This feature is robust in the NDIS data (it is not an artifact of the FT) and can be demonstrated not to be a consequence of the *Q*-range of the data obtained. It is possible that this difference is due to some shortcoming in the force fields used in the modeling.

Although the NDIS experimental evidence is compelling that strong ion pairing occurs in Gdm_2CO_3 and Gdm_2SO_4 solutions, these studies produced no direct experimental evidence to demonstrate that this pairing produced nanoscale ion clusters as was seen in the MD simulations. However, SANS is a widely used[19−23] and robust technique for unambiguously identifying intermediate-size structures since it is sensitive to regions of differing coherent scattering length density of approximately 1 nm and larger.

To quantify the average cluster size, the SANS data were fitted to the simplest form factor, monodisperse spheres.[24] Due to the unknown composition and density of clusters, a multiplicative scale factor and a flat, incoherent background were free parameters along with the sphere radius. The structureless incoherent scattering is effectively constant between these two samples because they have nearly identical constitutions. Since it is nearly impossible to calculate or measure this incoherent scattering, it has not been corrected for in these data. Instrumental smearing was included in the model fitting by smearing the model function but was not significant. The limited signal strength and scattering range precluded the use of more detailed models.

The results of the SANS experiments are presented in Figure 6. These measurements demonstrate that structures on the 1.6 nm length scale exist in the Gdm_2CO_3 solution, while no such structures exist in the GdmCl solution. Furthermore, it is unlikely that this marked difference in structuring behavior is an artifact of the different constitution of these solutions, as their atomic compositions are extremely similar (GdmCl = H, 0.646; O, 0.278; N, 0.045; C, 0.015; Cl, 0.015; $GdmCO_3$ = H, 0.637; O, 0.296; N, 0.044; C, 0.022). These results are consistent with those found from the NDIS experiments and MD simulations.[9]

Conclusions

The MD simulations reported here find a significant tendency for guanidinium and carbonate ions to pair in aqueous solutions.

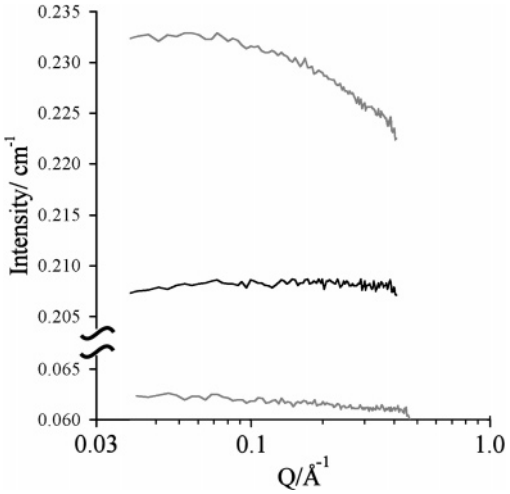

Figure 6. Small-angle neutron scattering of 1.5 M Gdm_2CO_3 (upper gray line) and 3 M GdmCl (black line). Also for comparison the SANS data for pure D_2O (lower gray line) are shown. The flatness of the GdmCl data shows that there is no coherent structure in this solution, while the Gdm_2CO_3 data are consistent with 1.6-nm-sized spherical aggregates in the solution.

These simulations predict that almost all of the ions in the Gdm_2CO_3 solution exist in nanometer-sized clusters held together by very strong hetero-ion pairing, even at the relatively modest concentration of 1.5 *m*. This simulation was used to design the most appropriate neutron scattering measurement to test the reliability of this predicted very strong ion pairing, uncluttered by the uninteresting correlations that tend to dominate the neutron scattering measurement. The parallel NDIS experiment confirmed that there is indeed very strong pairing in this system, similar to that found in the MD simulation.

Moreover, the NDIS results imply both from indicative smaller-angle scattering (0−1 Å^{-1} in $^n\Delta_N(Q)_{null}$) and from topological reasoning that nanometer-sized ion clusters exist in this solution. In strong agreement with the predictions of the MD simulations and the NDIS data, the SANS experiments directly confirm the presence of nanometer-sized structures in aqueous guanidinium carbonate solutions but not in solutions of guanidinium chloride.[9] Similar nanometer-scale ion aggregates have been suggested recently from dynamic light scattering experiments for solutions of $(NH_4)_2SO_4$ and sodium citrate.[25] Dielectric relaxation studies of aqueous $MgSO_4$ also found contact ion pairs and the possibility that such pairing may involve larger aggregates.[26] Cluster formation was also suggested in conductivity measurements for $(NH_4)H_2PO_4$ as early as the 1960s[27,28] and from Raman spectroscopy of $(NH_4)H_2PO_4$[29] and $NaNO_3$.[30] Given that the present study confirms the presence of mesoscale ion clusters in Gdm_2CO_3 solutions from both simulations and two additional experimental methods and that other studies find nanometer-scale clusters in Gdm_2SO_4 solutions as well,[10] the case for such aggregates in many electrolyte solutions appears to be quite strong. The case is even further strengthened by the observation that aggregates do not occur in all such solutions,[9] again in agreement with the simulation predictions.

The presence of ion clusters in some electrolyte solutions and not in others may also provide a mechanistic explanation for the ordering of the ions in the Hofmeister series.[1] While the Hofmeister ranking for monatomic cations correlates with surface charge density and solution surface tension, for complex polyatomic ions the underlying mechanisms for the Hofmeister series are less apparent.[31] For example, the guanidinium cation is an effective protein denaturant, while among anions, thiocy-

anate is a strong denaturant while sulfate stabilizes proteins. The differing effects of ions on proteins have long been attributed to changes that they were thought to induce in the collective structure of liquid water, with some ions labeled structure makers, or kosmotropes, and others described as structure breakers, or chaotropes. Although vague and nondescriptive, such terms are still in use, even though recent studies have not necessarily supported this simple picture.[31−34] Instead it appears that solutes structure those water molecules with which they directly interact in their hydration shells,[33,35,36] but the effects on more distant bulk water molecules appear to be much less significant.[32] Considering the very different clustering behavior of the thiocyanate and sulfate ions it may be that the ordering of these ions in the Hofmeister series has little do with the structuring that the ions impose upon water and instead is almost entirely due to the interactions of the ions with each other and with the protein.

The carbonate ion is not usually incorporated into the Hofmeister series, since unlike many other salts, carbonate tends to have a strongly basic character that is the dominant factor in its behavior in protein solutions. Nonetheless, the observation of nanometer-sized clusters in Gdm_2CO_3 solution, similar to those predicted by the MD simulations of both the Gdm_2CO_3 and the Gdm_2SO_4 solutions,[10] reinforces the argument that ion−ion interactions may be the key to understanding the Hofmeister series. The discovery of ion clusters of comparable length scale to the proteins themselves is surprising and in addition may account for much of the nonideal behavior of electrolytes for properties such as density, conductivity, diffusion, etc.

Acknowledgment. The authors gratefully acknowledge the assistance of G. Cuello and P. Palleau of the ILL. This project was supported by Grant No. GM63018 from the National Institutes of Health and by the National Science Foundation under Agreement No. DMR-9986442. The authors thank J. E. Enderby and M.-L. Saboungi for helpful discussions.

Supporting Information Available: Movie depicting the starting coordinates for the MD simulation and a representative snapshot from the equilibrated dynamics. This material is available free of charge via the Internet at http://pubs.acs.org.

References and Notes

(1) Hofmeister, F. *Arch. Exp. Pathol. Pharmakol.* **1888**, *24*, 247.
(2) Baldwin, R. L. *Biophys. J.* **1996**, *71*, 2056.
(3) Kaushik, J. K.; Bhat, R. *J. Phys. Chem. B* **1998**, *102*, 7058.
(4) Leberman, R.; Soper, A. K. *Nature* **1995**, *378*, 364.
(5) Sharp, K. A.; Madan, B.; Manas, E.; Vanderkooi, J. M. *J. Chem. Phys.* **2001**, *114*, 1791.
(6) Max, J.-J.; Chapados, C. *J. Chem. Phys.* **2001**, *115*, 2664.
(7) Enderby, J. E. *Chem. Soc. Rev.* **1995**, *24*, 159.
(8) Neilson, G. W.; Mason, P. E.; Ramos, S.; Sullivan, D. *Philos. Trans. R. Soc. London, Ser. A* **2001**, *359* (1785), 1575.
(9) Mason, P. E.; Neilson, G. W.; Enderby, J. E.; Saboungi, M.-L.; Dempsey, C. E.; MacKerell, A. D.; Brady, J. W. *J. Am. Chem. Soc.* **2004**, *126*, 11462.
(10) Mason, P. E.; Dempsey, C. E.; Neilson, G. W.; Brady, J. W. *J. Phys. Chem. B* **2005**, *109*, 24185.
(11) Schmidt, M. W.; Baldridge, K. K.; Boatz, J. A.; Elbert, S. T.; Gordan, M. S.; Jensen, J. H.; Koseki, S.; Matsunaga, N.; Nguyen, K. A.; Su, S.; Windus, T. L.; Dupuis, M.; Montgomery, J. A. *J. Comput. Chem.* **1993**, *14*, 1347.
(12) Jorgensen, W. L.; Chandrasekhar, J.; Madura, J. D.; Impey, R. W.; Klein, M. L. *J. Chem. Phys.* **1983**, *79*, 926.
(13) Brooks, B. R.; Bruccoleri, R. E.; Olafson, B. D.; Swaminathan, S.; Karplus, M. *J. Comput. Chem.* **1983**, *4*, 187.
(14) van Gunsteren, W. F.; Berendsen, H. J. C. *Mol. Phys.* **1977**, *34*, 1311.
(15) Darden, T.; York, D.; Pedersen, L. *J. Chem. Phys.* **1993**, *98*, 10089.
(16) Squires, G. L. *Introduction to the Theory of Thermal Neutron Scattering*; Cambridge University Press: Cambridge, U. K., 1978.
(17) Barnes, A. C.; Hamilton, M. A.; Beck, U.; Fischer, H. E. *J. Phys.: Condens. Matter* **2000**, *12*, 7311.
(18) Glinka, C. J.; Barker, J. G.; Hammouda, B.; Krueger, S.; Moyer, J. J.; Orts, W. J. *J. Appl. Crystallogr.* **1998**, *31*, 430.
(19) Mangiapia, G.; Berti, D.; Baglioni, P.; Teixeira, J.; Paduano, L. *J. Phys. Chem. B* **2004**, *108*, 9772.
(20) McLeish, T. C. B.; Allgaier, J.; Bick, D. K.; Bishko, G.; Biswas, P.; Blackwell, R.; Blottiere, B.; Clarke, N.; Gibbs, B.; Groves, D. J.; Hakiki, A.; Heenan, R. K.; Johnson, J. M.; Kant, R.; Read, D. J.; Young, R. N. *Macromolecules* **1999**, *32*, 6734.
(21) Finney, J. L.; Bowron, D. T.; Daniel, R. M.; Timmins, P. A.; Roberts, M. A. *Biophys. Chem.* **2003**, *105*, 391.
(22) Almásy, L.; Jancsó, G. *J. Mol. Biol.* **2004**, *113*, 61.
(23) Sullivan, D. M.; Neilson, G. W.; Fischer, H. E.; Rennie, A. R. *J. Phys.: Condens. Matter* **2000**, *12*, 3531.
(24) Roe, R.-J. *Methods of X-ray and Neutron Scattering in Polymer Science*; Oxford Press: New York, 2000.
(25) Georgalis, Y.; Kierzek, A. M.; Saenger, W. *J. Phys. Chem. B* **2000**, *104*, 3405.
(26) Buchner, R.; Chen, T.; Hefter, H. G. *J. Phys. Chem. B* **2004**, *108*, 2365.
(27) Mullin, J. W.; Raven, K. D. *Nature* **1961**, *190*, 251.
(28) Mullin, J. W.; Raven, K. D. *Nature* **1962**, *195*, 35.
(29) Ceretta, M. K.; Berglund, K. A. *J. Cryst. Growth* **1987**, *84*, 577.
(30) Rusli, I. T.; Schrader, G. L.; Larson, M. A. *J. Cryst. Growth* **1989**, *97*, 345.
(31) Breslow, R.; Guo, T. *Proc. Natl. Acad. Sci. U.S.A.* **1990**, *87*, 167.
(32) Omta, A. W.; Kropman, M. F.; Woutersen, S.; Bakker, H. J. *Science* **2003**, *301*, 347.
(33) Mason, P. E.; Neilson, G. W.; Barnes, A. C.; Enderby, J. E.; Brady, J. W.; Saboungi, M.-L. *J. Chem. Phys.* **2003**, *119*, 3347.
(34) Sidhu, K. S.; Goodfellow, J. M.; Turner, J. Z. *J. Chem. Phys.* **1999**, *110*, 7943.
(35) Schmidt, R. K.; Karplus, M.; Brady, J. W. *J. Am. Chem. Soc.* **1996**, *118*, 541.
(36) Liu, Q.; Brady, J. W. *J. Am. Chem. Soc.* **1996**, *118*, 12276.